



Universidad Autónoma
de Madrid

Biblos-e Archivo
Repositorio Institucional UAM

Repositorio Institucional de la Universidad Autónoma de Madrid

<https://repositorio.uam.es>

Esta es la **versión de autor** del artículo publicado en:
This is an **author produced version** of a paper published in:

Journal of Materials Science 55.13 (2020): 5458-5470

DOI: <https://doi.org/10.1007/s10853-020-04394-z>

Copyright: © 2020 Springer Science+Business Media, LLC, part of Springer Nature

El acceso a la versión del editor puede requerir la suscripción del recurso

Access to the published version may require subscription

Hybrid porous silicon/silver nanostructures for the development of enhanced photovoltaic devices

Rehab Ramadan^{1,2,*}, Miguel Manso-Silván^{1,3}, and Raúl J. Martín-Palma^{1,3}

¹ Departamento de Física Aplicada, Universidad Autónoma de Madrid, Campus de Cantoblanco, 28049 Madrid, Spain.

² Department of Physics, Faculty of Science, Minia University, 61519, Minia, Egypt.

³ Instituto Universitario de Ciencia de Materiales “Nicolás Cabrera” (INC), Universidad Autónoma de Madrid, Campus de Cantoblanco, 28049 Madrid, Spain

*Corresponding author Email address: rehab.ramadan@predoc.uam.es

ABSTRACT

Si-based metal-insulator-semiconductor (MIS) Schottky-junction solar cells with the basic structure Al/Si/TiO₂/Au were fabricated. This structure was modified by the addition of nanostructured porous silicon (nanoPS) layers and silver nanoparticles (AgNPs), resulting in devices with the following structures: Al/Si/nanoPS/TiO₂/Au and Al/Si/nanoPS+AgNPs/TiO₂/Au. The key performance parameters of the three MIS Schottky-junction solar cells were determined, including spectral photocurrent response, short-circuit current density, open-circuit voltage, fill factor, and efficiency. The experimental results show a remarkable enhancement in the overall performance of the solar cells upon the addition of nanoPS and AgNPs layers to the basic structure. An energy band model is proposed for the Si-based MIS Schottky junction solar cells to understand the different photogeneration and conduction mechanisms.

Keywords: MIS solar cell; Schottky junction; nanostructured porous silicon; optical absorption; silver nanoparticles; surface plasmon resonance; energy band diagrams; photocurrent response, efficiency.

1. INTRODUCTION

The unlimited availability of solar energy makes photovoltaic (PV) technology an inexpensive, renewable, clean, and reliable source of electricity generation for both space and terrestrial applications [1]. However, in spite of all the available alternatives and the intense research in this area, silicon is likely to remain the dominant PV material for the foreseeable future, given its abundance in the earth's crust, long-term stability, well-established technology (having its origins in the semiconductor industry), and relatively low cost [2]. However, crystalline silicon (c-Si) still has several drawbacks which limit its performance. These include optical losses and high recombination rates, as well as thermal and quantum losses [3]. Many efforts have been made by researchers to reduce optical losses and carrier recombination rates. In particular, various nanostructures were grown on Si substrates, including Si nanowires [4-6], quantum dots [7], and porous silicon [8], as well as periodic, random, and pyramidal surface texturing [9, 10].

A different approach to achieve an efficient photovoltaic conversion of solar energy goes through the development of metal-semiconductor (MS) Schottky junction solar cells based on c-Si, basically because of their structural simplicity and therefore convenient realization [11]. Moreover, these solar cells are inexpensive compared to solar cells based on diffused p-n junctions and they also overcome the issues related to high temperature diffusion. However, MS solar cells usually show lower conversion efficiencies compared to p-n junction solar cells of the same materials due to their typically low open-circuit voltage [12]. However, metal-insulator-semiconductor (MIS) junctions show increased open-circuit voltage due to tunneling through the insulating layer of the majority carriers or diffusion current due to the minority carriers [13, 14], thus improving the overall conversion efficiency of Schottky-barrier solar cells.

In the present work, we present our findings related to the study of the optoelectronic performance of three different MIS Schottky junction solar cells. These include a device with the structure Al/Si/TiO₂/Au and two modified devices. The first variation includes a nanoporous silicon (nanoPS) layer, leading to the structure Al/Si/nanoPS/TiO₂/Au, while

the second one includes silver nanoparticles (AgNPs) embedded into the nanoPS layer, leading to the structure Al/Si/nanoPS+AgNPs/TiO₂/Au.

The modified devices constitute two strategies which are implemented to improve light absorption and minimizing the carrier recombination rates of c-Si. In the first variation (Al/Si/nanoPS/TiO₂/Au devices), nanoPS is used as a wideband optical absorber [15]. However, this choice has two main drawbacks: (i) the surface of nanoPS is rapidly oxidized upon exposition to the atmosphere, leading to changes in its optical properties [16], and (b) two main recombination mechanisms can take place on the surface of nanoPS, namely radiative recombination through surface states (surface recombination) and through oxygen vacancies [17]. In this line, thin layers of In₂O₃ [16], SiO₂ or SiO₂/SiN [18], TiO₂ [19] and Al₂O₃ or Al₂O₃/SiN have been used to passivate the surface of nanoPS [20]. Thin layers with high resistivity or even insulating nature in contact with the active layer of solar cells limit the amount of current that can flow into a small localized area, thus lowering the carrier mobility which improves cell efficiency as a result of an increase in the open-circuit voltage [21]. In particular, the use of TiO₂ thin films has the great advantage of serving at the same time as passivation layers to prevent nanoPS from oxidation and to increase the open-circuit voltage. At the same time, the TiO₂ thin films can be used as antireflective coatings [22].

In the second variation (Al/Si/nanoPS+AgNPs/TiO₂/Au devices), plasmonic effects are used to increase light absorption and short circuit current [23]. Furthermore, the immersion in noble metal ion solutions during the growth of metal nanoparticles is used to modify the surface properties of nanoPS [24-26]. Anyhow, although the use of plasmonic nanoparticles seems in principle attractive, it presents significant challenges. For instance, an excessive surface density of embedded nanoparticles in the active layer would increase carrier recombination rates and, as a result, decrease the overall solar cell efficiency [27].

The experimental results show a remarkable improvement in the photovoltaic performance of the Al/Si/nanoPS/TiO₂/Au devices. Furthermore, a notable enhancement in the photocurrent response of the devices based on nanoPS layers combined with metallic AgNPs has been measured.

2. EXPERIMENTAL

2.1 Fabrication of the active nanoPS layers

NanoPS layers were fabricated by the electrochemical anodization of boron doped (*p*-type) silicon wafers of <100> orientation, resistivity in the 25-30 $\Omega\cdot\text{cm}$ range, and surface roughness of the order of 0.1 nm. Al bottom contacts were deposited by electron beam evaporation. For the evaporation, the base pressure was 1.25×10^{-5} mbar and the evaporation time was 4 minutes, resulting in 150 nm-thick Al thin films. The Al thin films were subsequently annealed by rapid thermal processing (RTP) in nitrogen atmosphere for 5 minutes to turn the initial rectifying behavior into an ohmic one. Afterwards, the wafers were cut into $1.5\times 1.5\text{ cm}^2$ pieces. Each piece was mounted in a sample holder with an area of about 1.23 cm^2 exposed to the etching solution (the active area of the solar cell device). The etching solution consisting in a 1:6 HF (48 wt%):dimethyl formamide (99 wt%) mixture. Before the etching process, the native oxide layer was removed by immersing the Si substrates into HF:H₂O solutions (1:20 ratio) for 30 s. Next, the substrates were cleaned by immersion in acetone and ethanol and then distilled water to remove any residuals from the HF solution. The applied current density ranged between 5 and 15 mA/cm², leading to layers with different porosities and different dimensions of the nanopores. The anodization time was fixed at 120 s. After the fabrication process, each sample was rinsed in ethanol and blown dry with dry nitrogen. The experimental setup of the anodization process was schematically described in a previous work [15].

2.2 Infiltration of Ag NPs

The nanoPS layers were used as templates for the subsequent growth of silver nanoparticles. For this task, we used an electrochemical deposition process previously implemented [15] at a fixed current density of $1\mu\text{A}/\text{cm}^2$ and a fixed duration of 4 minutes (without optimization of the density of the infiltrated nanoparticles). The aqueous solution was composed of silver nitrate, sodium citrate and nitric acid, with pH=3. This process led to the formation of hybrid nanoPS/Ag NPs layers.

2.3 Spin coating of TiO₂ thin films

A solution of titanium isopropoxide (Ti[OCH(CH₃)₂]₄) in ethanol was prepared with a 0.4 M concentration. Next, 0.35 M concentration of HCl acid were added to the solution to induce an acid catalysis to prevent nanoPS from damage [28]. The solution was stirred at 3000 rpm at room temperature for 30 minutes to obtain a clear solution. 60 µL of the sol were cast on either the Si substrate, nanoPS layer or the nanoPS+AgNPs hybrid layer at a spinning speed of 3000 rpm for 30 s. Finally, the resulting TiO₂ thin films were annealed on a hot plate at 150°C for 5 minutes to evaporate the remaining solvents.

Furthermore, aiming at determining the energy bandgap of TiO₂ thin films from optical absorption measurements, 60 µl of TiO₂ sol were cast on clean glass substrates at the same previous spinning speed and for the same time.

2.4 Fabrication of Au micropatterned top contact by UV Lithography

A negative photoresist (Ariston 20 series) was used for the lithographic process on the Au thin films as previously described [29]. The Au thin films were deposited using a DC sputtering system in argon atmosphere. The typical deposition pressure was 2×10^{-2} mbar and the typical plasma current 20 mA, leading to a thickness of around 90 nm. The photoresist spin time was 30 seconds and the spin speed was 4000 rpm. Afterwards, the samples were dried on a hot plate at 70°C for 15 minutes. The photoresist/Au film stack was then exposed to UV radiation (Hamamatsu LC-L1 UV-led spot light source, $1 \text{ W} \times \text{cm}^{-2}$) through a printed photo mask for 3 minutes. The photoresist micropattern was subsequently developed by immersing the sample in a 0.25 M NaOH solution for 1 minute. Next, any residuals from the Au thin film were removed by wet etching, i.e., by immersing the sample in HCl: HNO₃ (1:3) solution for 1 minute. The photoresist was finally lift-off in acetone and afterwards the device was cleaned using ethanol and distilled water, and dried in nitrogen.

An illustration of the final structure of the different devices is presented in Fig. 1, including FESEM images of the active layer/TiO₂ interfaces, where the active layers are Si, Si/nanoPS, and Si/nanoPS+AgNPs, leading to devices with the following structures:

Al/Si/TiO₂/Au, Al/Si/nanoPS/TiO₂/Au, and Al/Si/nanoPS+AgNPs/TiO₂/Au, respectively. In addition to a real top-view image of the fabricated devices.

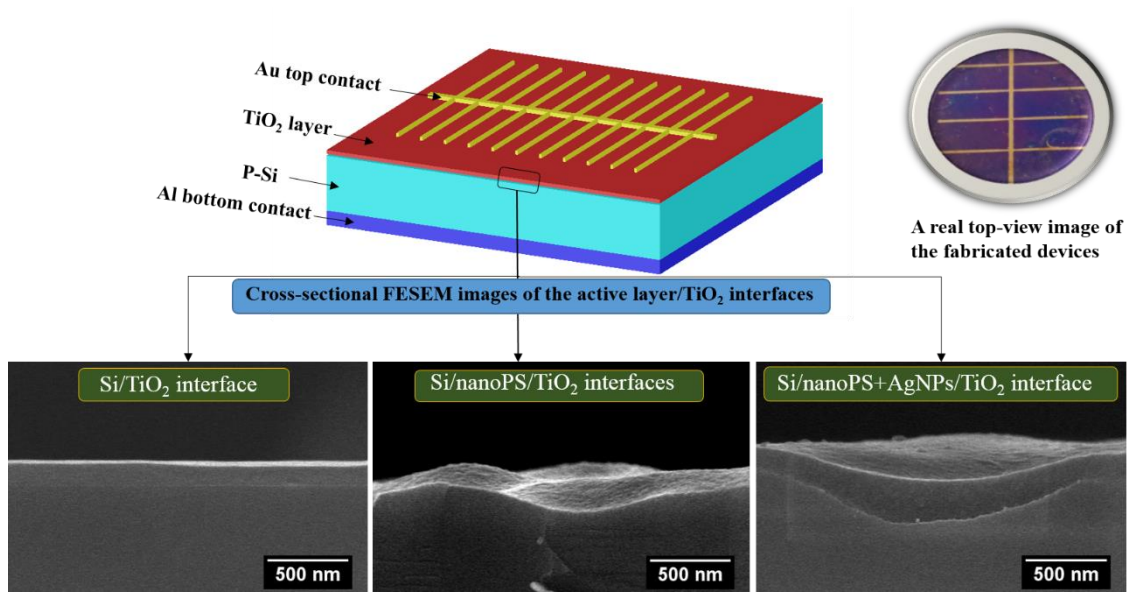


Figure 1: Schematic illustration of the structure of the Schottky junction solar cell devices fabricated for this study, with FESEM cross-sectional images of the active layer/TiO₂ interfaces for the three devices. In addition to a real top-view image of the fabricated devices.

2.5 Characterization techniques

The morphology of the thin films and interfaces was studied by field emission scanning electron microscopy (FESEM) using a Philips XL- 40FEG microscope operated at 5 kV. Optical characterization in the UV-visible range (250-900 nm) was carried out using a Jasco V-560 double-beam spectrophotometer, equipped with an integrating sphere to avoid scattering losses.

The electrical characterization of the MIS Schottky junction solar cells was carried out in a Bio- Logic SP-150 potentiostat with a scan rate 5 mV/s and applied potential in the +1.5 to -1.5 V range. A homemade cell consisting of two movable copper probes with a diameter of 0.5 mm and a copper base (2×2 cm²) was used. The measurements were carried out in a Faraday box to shield them from any external signals.

A solar simulator (LCS-100 Solar Simulator-Model 94011A), with a calibrated illumination power density of 100 mW/cm^2 was used as the light source to measure the photovoltaic characteristics of the fabricated MIS Schottky solar cells.

Photocurrent measurements were carried out at 0 V bias using a dual digital lock-in amplifier (Signal Recovery 7225) at a chopper frequency of 300 Hz. Illumination was provided by an Acton Research Corporation Tungsten-Deuterium dual light source (model TDS-429) and a SpectraPro 150 monochromator equipped with three interchangeable diffraction gratings (1200 lines/mm) was used to select the wavelength.

3. EXPERIMENTAL RESULTS

3.1 Morphology

The FESEM images portrayed in Fig. 2 show the different layers which compose the final devices. More specifically, Figs. 2(a) and 2(b) show the microstructure of the nanoPS layers and demonstrate the presence of AgNPs inside its pores and on the surface. Besides, it is observed that the nanoPS layers comprise macro-pores, with typical diameters in the 500 to 600 nm range, combined with meso-pores with diameters in the 5 to 30 nm range. Furthermore, the diameter of the AgNPs typically ranges between 5 and 15 nm. A cross-sectional view of the Si/nanoPS+AgNPs/TiO₂ interface is depicted in Fig. 2(c), from which the thickness of the nanoPS layer was determined to be around 120 nm. Spin coating of TiO₂ sol-gel leads to the filling of the nanopores with the sol and the formation of very thin films (~10 nm) over the nanoPS layers, as shown in Fig. 2(c). The wavy shape of the top surface of the devices, portrayed in Fig. 2(d), confirms the extremely low thickness of the TiO₂ interfacial thin film, which grows conformably following the underlying structure of the nanoPS layer. Likewise, the top Au metallic contact, with a thickness around 90 nm, follows the wavy surface shape of the TiO₂ thin film, as presented in Fig. 2(d).

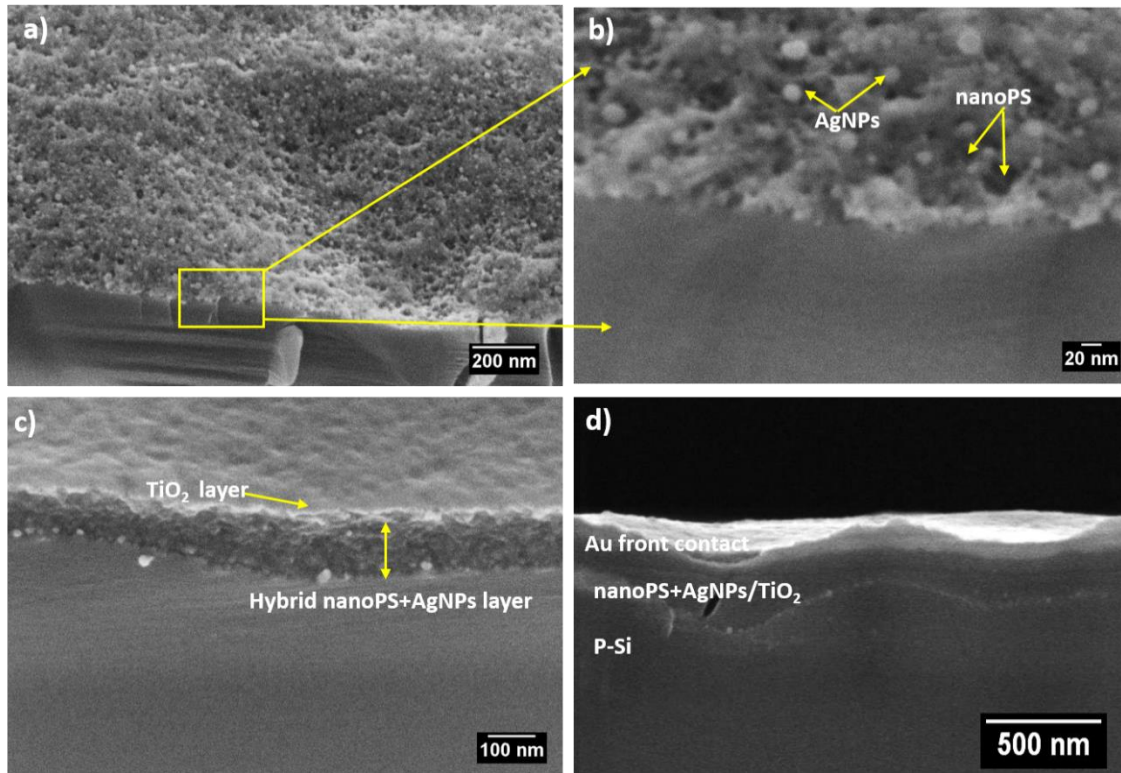


Figure 2: (a) Top view FESEM images of a typical hybrid nanoPS+AgNPs layer, (b) high magnification image of a hybrid nanoPS+AgNPs layer. (c) Cross-sectional view showing a TiO_2 thin film grown onto the nanoPS+AgNPs layer. (d) Cross-sectional image of the Si/nanoPS+AgNPs/ TiO_2 /Au structure.

3.2 Optical properties

3.2.1. Reflectance spectra

In general terms, nanoPS may be described as a homogeneous mixture of silicon nanocrystallites, amorphous silicon, and air (pores), with typical feature sizes well below the wavelength of infrared and visible light [30, 31]. Thus, in this wavelength range, the optical properties of nanoPS will mainly depend on the composition of this mixture [32]. In this section, we analyze the effect of porosity on the overall reflectance (R) spectra of the nanoPS layers grown onto Si. Fig. 3 shows the reflectance spectra of Si and of three different nanoPS layers grown onto the Si substrate. From the experimental results, it is evident that the growth of nanoPS layers onto Si results in a significant reduction of the average reflectance. It is particularly remarkable that the average reflectance in the 250 to 900 nm wavelength range decreases from 35% to 19% for anodization current densities increasing from 5 mA/cm^2 to 15 mA/cm^2 (the average reflectance for the Si substrate is 41 %). In particular, a drastic reduction of R for wavelengths shorter than 400 nm is clearly observed. As pointed out before, this effect has its origin in a reduction of the

effective index of refraction of the nanoPS layers with increasing porosity, i.e., increasing anodization current density. At the same time, increased porosity and reduced crystallite size results in increased transparency.

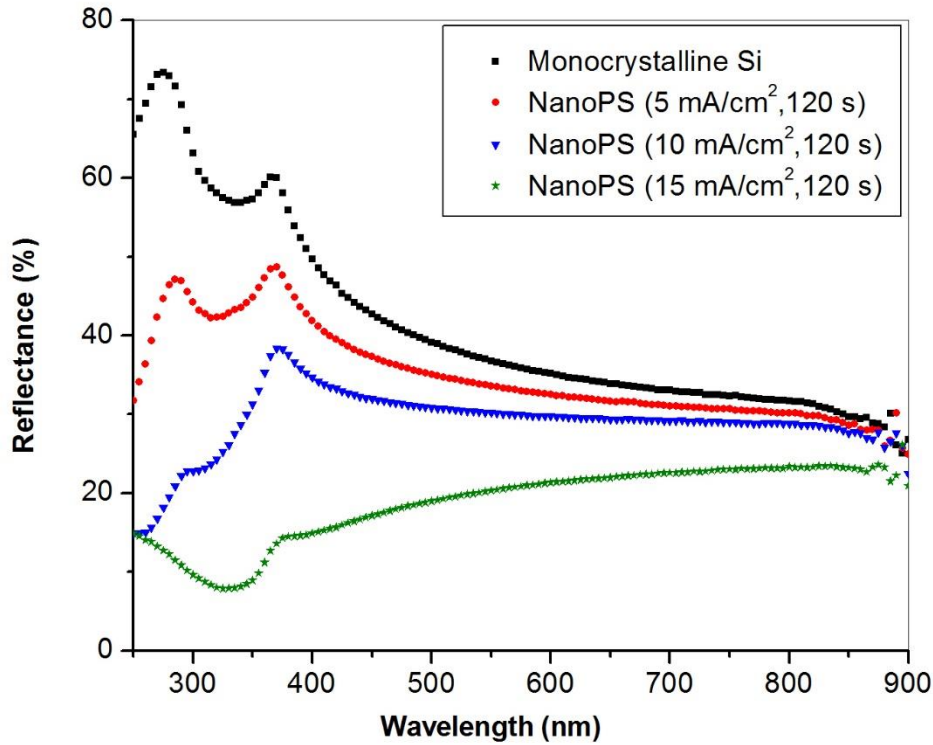


Figure 3. Overall reflectance spectra of bulk Si and nanoPS layers grown onto Si substrates under different etching current densities (5, 10, and 15 mA/cm²) and at a fixed anodization time (120 s).

The experimental results allowed us to select an anodization current density of 10 mA/cm² as the best compromise between reflectance reduction and electrical conductivity (studied in a previous work [33] for the subsequent fabrication of the photovoltaic devices. This particular current density leads to nanoPS layers with a porosity of 60.3% and quite low values of average reflectance (29% in the 250 to 900 nm wavelength range). Furthermore, a relatively small decrease in the electrical conductivity, as determined from AC and DC electrical characterization [33].

Figure 4 shows the reflectance spectra of the Si substrate and the following layers grown onto Si: nanoPS, nanoPS+AgNPs, TiO₂/nanoPS, and TiO₂/nanoPS+AgNPs. It is clearly observed that the infiltration of silver nanoparticles into the nanoPS layers resulted in

increased reflectance, especially in the UV-visible region. It is well known that the presence of noble metal nanoparticles leads to the generation of surface plasmon resonances (SPRs) which would reduce or shift the transmittance and/or reflectance spectra [34]. As such, metal NPs usually enhance the efficiency of photovoltaic devices by reducing reflection and increasing light trapping within the device. However, the specific optical behavior depends on the density of NPs, as well as their shape and size [35]. In some cases, the presence of metal NPs results in high reflectivity due to the backscattering of the NPs itself, or due to a large surface density of nanoparticles, which can reach their percolation threshold and even form a quasi-continuous thin film [36, 37]. Nevertheless, a large surface density of nanoparticles would result in improved electrical conduction. As such, aiming at reducing the reflectance produced by the metal NPs without decreasing their density, which has a favorable effect on the electrical conduction, very thin layers of TiO_2 (~10 nm) were deposited over the hybrid nanoPS+AgNPs layers. TiO_2 was used given its low optical absorption in the visible [38].

The experimental results, portrayed in Fig. 4, confirm that depositing thin films of TiO_2 onto both nanoPS and nanoPS+AgNPs layers has a notable effect in reducing R . As such, the average reflectance in the 250 to 900 nm wavelength interval decreased from 29% to 14% upon deposition of TiO_2 thin films on the nanoPS layer and from 35% to 16 % on the nanoPS+AgNPs hybrid layers.

Focusing on the average R of the devices with the structures $\text{Al/Si/nanoPS/TiO}_2/\text{Au}$ and $\text{Al/Si/nanoPS+AgNPs/TiO}_2/\text{Au}$, a slight increment (from 14% to 16%) was observed upon the growth of silver NPs. However, the addition of metallic AgNPs to the nanoPS layers results in a notable reduction of the average reflectance (from 23.8% to 17.5%) in the blue region of the optical spectrum ($\lambda=250\text{-}450$ nm). Thereby, we claim that SPR effects occur in this region which are attributed to the small size of the AgNPs (between 5 and 15 nm) [39].

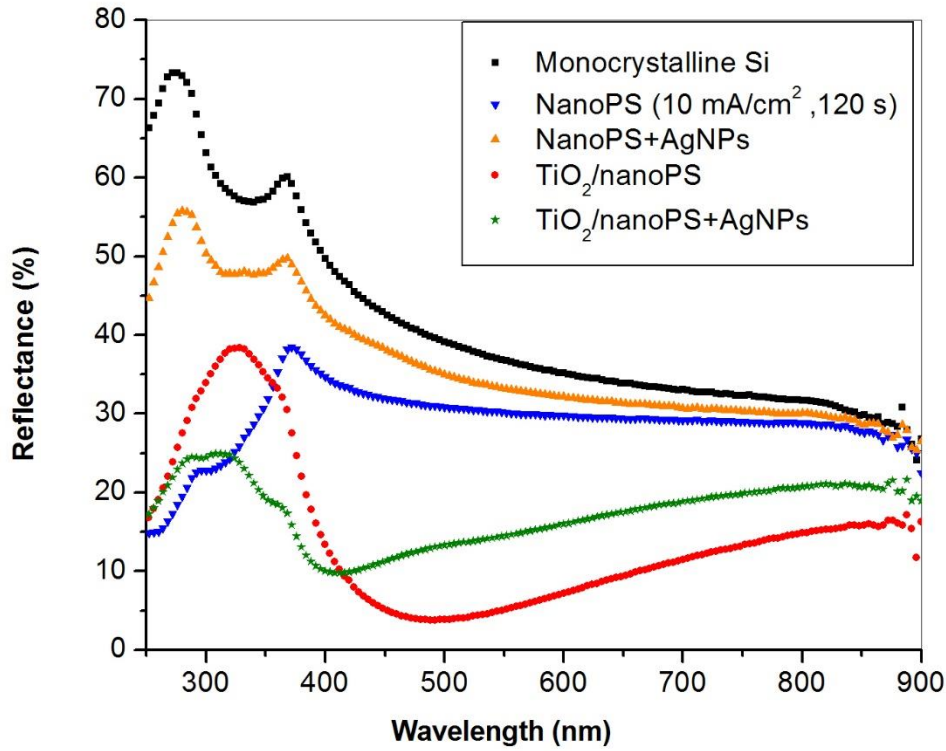


Figure 4. Overall reflectance spectra of bulk Si, nanoPS layers grown at 10 mA/cm² for 120 seconds, nanoPS+AgNPs layers (infiltrated at 1 μ A/cm² for 4 minutes), TiO₂/nanoPS layers, and TiO₂/nanoPS+AgNPs layers. All the structures were grown onto Si substrates.

3.2.2. Determination of the bandgap of the TiO₂ thin films

In addition to reducing reflectance, the TiO₂ thin films in the MIS Schottky junction solar cells serve as interfacial layers. Accordingly, determining their energy band gap (E_g) is a key step to create an energy band diagram for the devices. This would also allow us to analyze the electrical conduction mechanisms.

The optical bandgap of the TiO₂ thin films can be determined from Tauc plots [40]. First, the spectral behavior of the absorption coefficient (α) was calculated from the optical measurement, afterwards, the relationship between $(\alpha \cdot d)^2$ and the photon energy was plotted (Fig. 5), where d is the thickness of the TiO₂ thin films. By assuming that the TiO₂ thin films show a direct band gap character [41], its band gap can be calculated by extrapolating the straight line of the relationship between $(\alpha \cdot d)^2$ and the photon energy ($h\nu$), as shown in Fig. 5. The value of E_g for the TiO₂ thin films was found to be 3.82 eV.

This value is in good agreement with previous results obtained for TiO₂ thin films prepared by the sol gel method [41] and by sputtering [42].

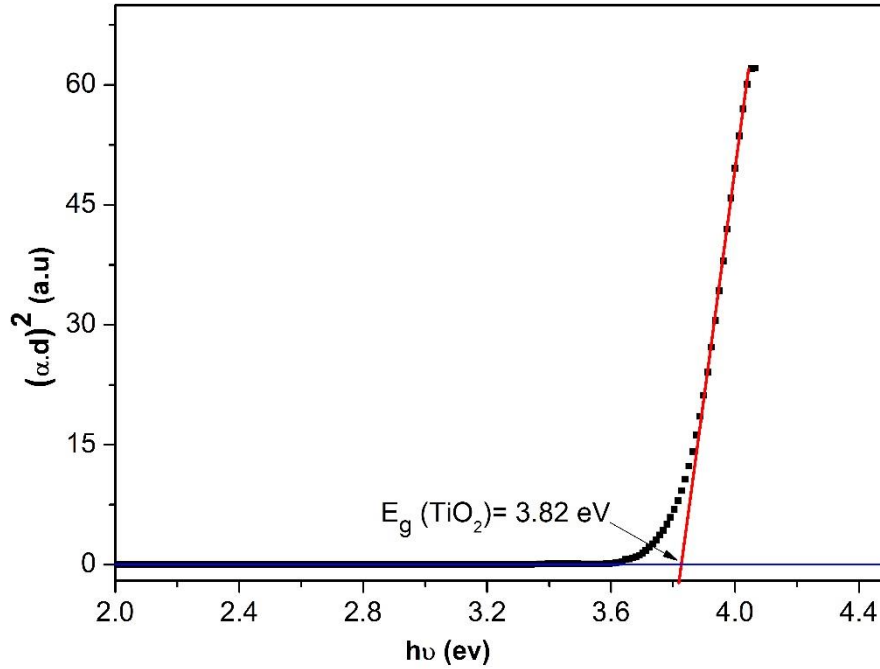


Figure 5: Tauc plot for TiO₂ thin film deposited on a glass substrate to determine its E_g value.

3.3 Energy band diagrams

Energy band diagrams allow understanding the electronic and optoelectronic behavior of Schottky junctions. Figure 6 shows the energy band diagrams that we propose for the three different MIS Schottky junction devices under study. In all cases, the TiO₂ thin films, given their small thickness, behave as tunneling interfacial regions between the active layer and the front Au contact [43]. Although there are different forms of TiO₂, all of them are semiconductors with empty and filled band edges at ~ 4.0 eV and 7.9 eV below the vacuum level, as shown in Fig. 6 [43]. The electron affinity at the surface of Si (100) is about 4.05 eV and the valence band edge is located at around 5.17 eV below the vacuum level [43]. Anyhow, it is important to keep in mind that these values would slightly change due to the particular processes and techniques used for the fabrication of the different layers.

Accordingly, in the case of the Al/Si/TiO₂/Au structures (Fig. 6(a)), the interface between Si and TiO₂ is expected to have a large valence band barrier ($\Delta E_v \sim 2.5$ eV), which would block the transportation of holes from Si to TiO₂ and would only allow the transportation of minority carriers (electrons) to the Au contact, where the electron conductivity must be large and the hole conductivity must be low. Majority carriers (holes) move to the rear contact of the solar cell to increase the hole conductivity, where the hole conductivity is large and the electron conductivity is low (Al contact). In all, the valence band offset (ΔE_v) between Si and the TiO₂ thin film allows using the TiO₂ interlayer at the same time for electron harvesting and hole blocking to the Au contact. As a result, surface recombination is minimized, while the open-circuit voltage increases [43]. Regarding the interfacial layer in the MIS Schottky junctions, a very thin film is the best option to avoid increasing the series resistance of the device. That would lead to a decrease in the fill factor and the overall efficiency of the solar cells [12] in the case of the Al/Si/TiO₂/Au structures (Fig. 1). The main reasons for photoresponse reduction for this device are discussed in detail in section 3.4.1.

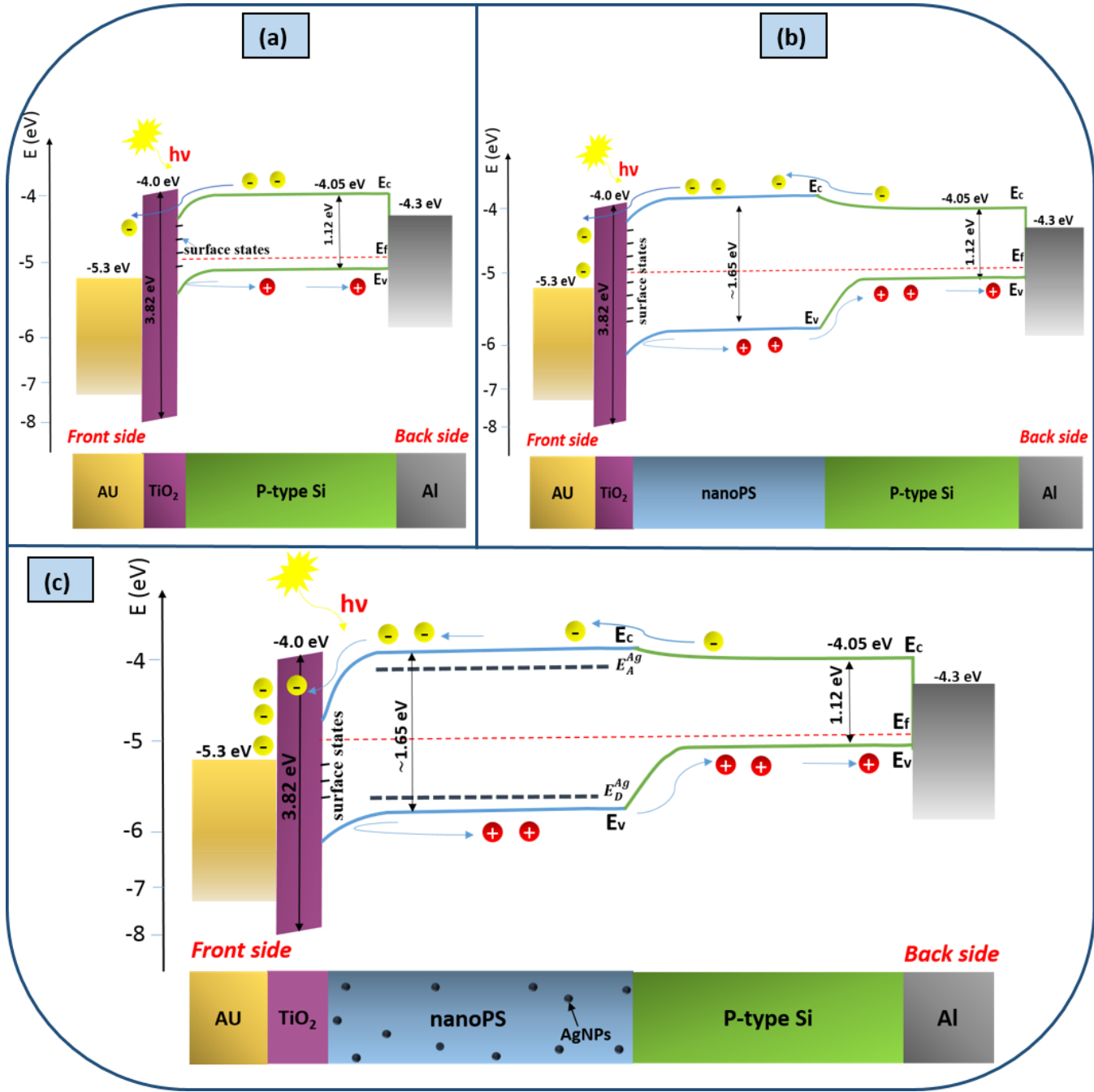


Figure 6. Illustration of the proposed energy band diagrams for the different Si-based Schottky solar cells, namely (a) Al/Si/TiO₂/Au devices, (b) Al/Si/nanoPS/TiO₂/Au devices, and (c) Al/Si/nanoPS+AgNPs/TiO₂/Au devices, with indication of surface states.

Figure 6(b) shows the proposed energy band diagram corresponding to MIS Schottky devices with the structure Al/Si/nanoPS/TiO₂/Au. The Fermi level for nanoPS is located close to the middle of the energy gap [44, 45] as a consequence of the formation of pores at defects and dopant sites of Si [16, 44, 46], thereby considerably reducing the doping concentration of Si

and widening the energy gap of PS with respect to that Si (its energy band gap is 1.12 eV) [47]. We estimate the energy band gap value of nanoPS to be around 1.65 eV, corresponding to a porosity of 60.3% [47, 48]. Deposition of TiO₂ on the nanoPS layers has the important effect of reducing the rate of the different recombination mechanisms. Two primary competing recombination mechanisms are possible after the fabrication of nanoPS on Si, namely radiative recombination through the surface states (surface recombination) and radiative recombination through the oxygen vacancies [17]. This way, passivating the surface of nanoPS leads to an enhancement of the generation of electron/hole pairs by reducing the surface recombination rates. However, as previously shown (see section 3.1), nanoPS comprises pores of dimensions at two very different scales, i.e., macro- and meso-pores. Coating nanoPS with TiO₂ results in an effective coverage of the macro-pores with the sol. However, the meso-pores may still have oxygen vacancies given their small dimensions with typical diameters in the 5-30 nm range (see FESEM images in Fig. 2). Accordingly, radiative recombination processes through the oxygen vacancies in the meso-pores may still take place. For this reason, in addition to using TiO₂ thin films, chemical interaction with noble metal ions during the growth of the silver NPs has been used to further passivate the surface of nanoPS.

Figure 6(c) shows the proposed energy band diagram after growing AgNPs into the nanoPS layers. Given the small size and low surface density of the silver nanoparticles and based on previous experiments with Ag-doped Si [49], we hypothesize that the presence of the AgNPs leads to donor and acceptor levels in the forbidden region of nanoPS. According to this assumption, the addition of silver to the porous layers results in a singly ionized donor level in the lower half of the forbidden band of nanoPS (E_D^{Ag}) and an acceptor level in the upper half of the forbidden band of nanoPS (E_A^{Ag}). These ionized levels might lead to increased generation of electron-hole pairs by capture and emission of carriers in the nanoPS+AgNPs layer.

In the case of the Al/Si/nanoPS+AgNPs/TiO₂/Au structures, we claim that the optoelectronic enhancement is due to four mechanisms. (1) Increased light absorption by the nanoPS layers in addition to TiO₂ thin films acting as antireflective coatings and passivating layers. (2) Improved surface passivation during the infiltration of the Ag NPs. (3) SPR effects at the interface between the metallic AgNPs and the TiO₂ and nanoPS layers manifested in the blue region of the electromagnetic spectrum (Fig. 4). Moreover, the generation of electron/hole

pairs is greatly enhanced due to the electrical enhancement in the active layer by the AgNPs.
(4) Improved electrical conduction given by the presence of silver nanoparticles.

3.4 Photovoltaic properties

3.4.1. Photocurrent response characterization

Figure 7 shows the photocurrent response in the 300-1200 nm wavelength range for the three MIS Schottky junction devices studied in this work. The experimental results show that the photocurrent presents a remarkable increase over all the wavelength range due to the incorporation of nanoPS layers, TiO₂ dielectric thin films, and the infiltration of silver nanoparticles into the porous structure. First, for the Al/Si/TiO₂/Au MIS Schottky junction solar cells, the photocurrent is very small, with values in the range of 10⁻¹¹ A. The small photocurrent levels for this device are attributed to three main reasons, namely (1) the indirect band gap character of Si, which causes an increase of the carrier recombination rates [3, 50], (2) a thicker TiO₂ thin film than in the other devices, because flat Si accepts more TiO₂ sol during spin casting due to surface tension and fluidics, as previously presented in Fig.1, and (3) large reflectance losses at the Si surface, especially at lower wavelengths. The photovoltaic performance of the device was improved by growing nanoPS layers, which led to a radical decrease in the average reflectance from 41% (Si substrate) to 29% for the nanoPS/Si structure (see section 3.2.1). However, texturing the surface of Si causes an increase number of defects on the surface, leading to increased recombination rates in addition to conduction losses [51]. However, the infiltration of Ag nanoparticles inside the nanoPS layers results in a drastic enhancement in the photocurrent response by three orders of magnitude.

Three main reasons might be behind this remarkable improvement. (1) The resonant oscillation of conduction electrons (SPR) in the blue region of the electromagnetic spectrum. The SPR effect is stimulated by the incident light at the interface between the metallic nanoparticles (AgNPs) and the dielectric films (TiO₂ thin layers), which have negative and positive permittivity. The intensity of the resonances is determined by the dielectric properties of the metal and the surrounding medium and by the particle size and shape [39]. The large enhancement in the near UV-blue region is attributed to the small size of the AgNPs (diameters in the 5 to 15 nm range), leading to higher absorption (Fig. 4) and generation of electron/hole pairs. (2) Surface passivation of nanoPS is improved

during the growth of the AgNPs by reducing the radiative recombination induced by oxygen vacancies in the meso-pores. (3) The electrical conduction of nanoPS is highly improved by the presence of the metallic nanoparticles, as previously discussed for Au NPs [2]. From our recent study on the AC and DC electrical properties of these structures, a large enhancement in the diffusion length of the minority carriers was found, which led to improving carrier separation and generation of electron/hole pairs [33].

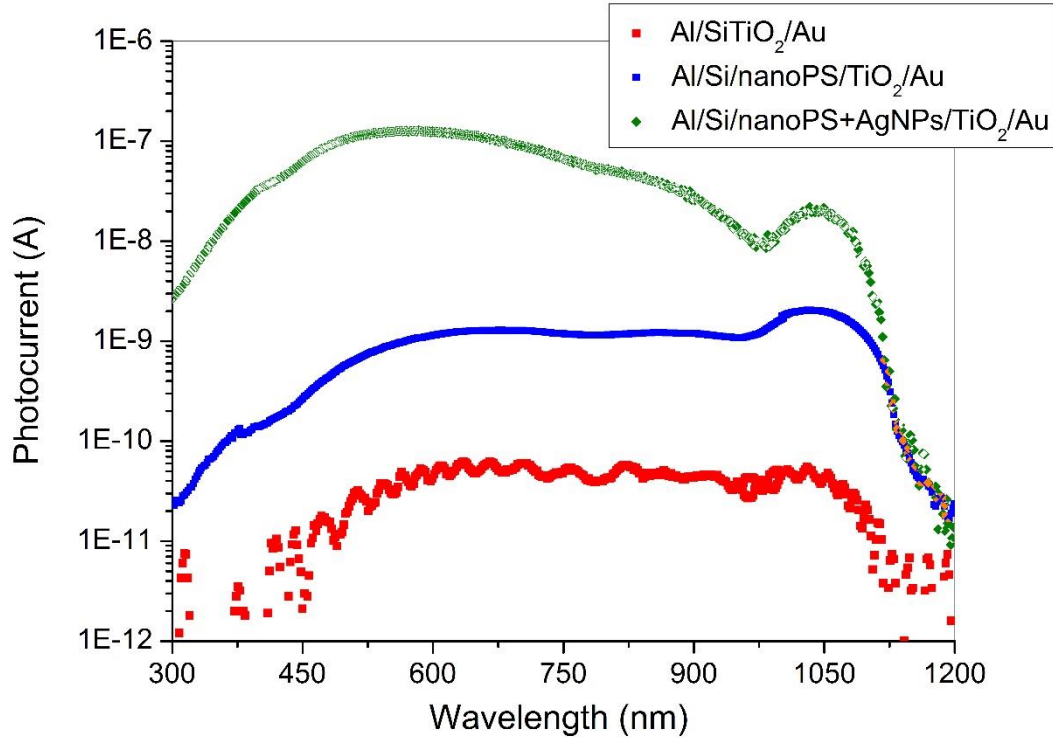


Figure 7. Spectral photocurrent response in the 300 to 1200 nm wavelength range for the three MIS Schottky junction devices studied in this work.

3.4.2. Current-voltage characterization under illumination

The current density–voltage (J - V) characteristics of the three MIS Schottky junction solar cells under illumination (100 mW/cm^2) was measured. The experimental results are shown in Fig. 8. The different electrical parameters which characterize the performance of solar cells, i.e., open circuit voltage (V_{oc}), short circuit current density (J_{sc}), fill factor (FF), and conversion efficiency (η), were determined from the experimental J - V curves and are presented in Table 1. A remarkable enhancement of both V_{oc} and J_{sc} for the Al/Si/nanoPS/TiO₂/Au Schottky barrier devices when compared to the Al/Si/TiO₂/Au

devices is observed, most likely due to reduced reflectance losses provided by the porous structure. Also, filling the nanopores with the TiO_2 sol led to decreasing its thickness, making these thin films more suitable as interfacial layers for the MIS solar cells. It is also noticeable that electron/hole-pair generation is drastically improved by the infiltration of AgNPs into the nanoPS layers, probably due to the combined action of SPR effects, the reduction in R , and increased conduction, as discussed in section 3.4.1. As a result, the conversion efficiency (η) increased from 0.9% for the $\text{Al/Si/nanoPS/TiO}_2/\text{Au}$ devices up to 1.9% for the $\text{Al/Si/nanoPS+AgNPs/TiO}_2/\text{Au}$ structures (Table 1).

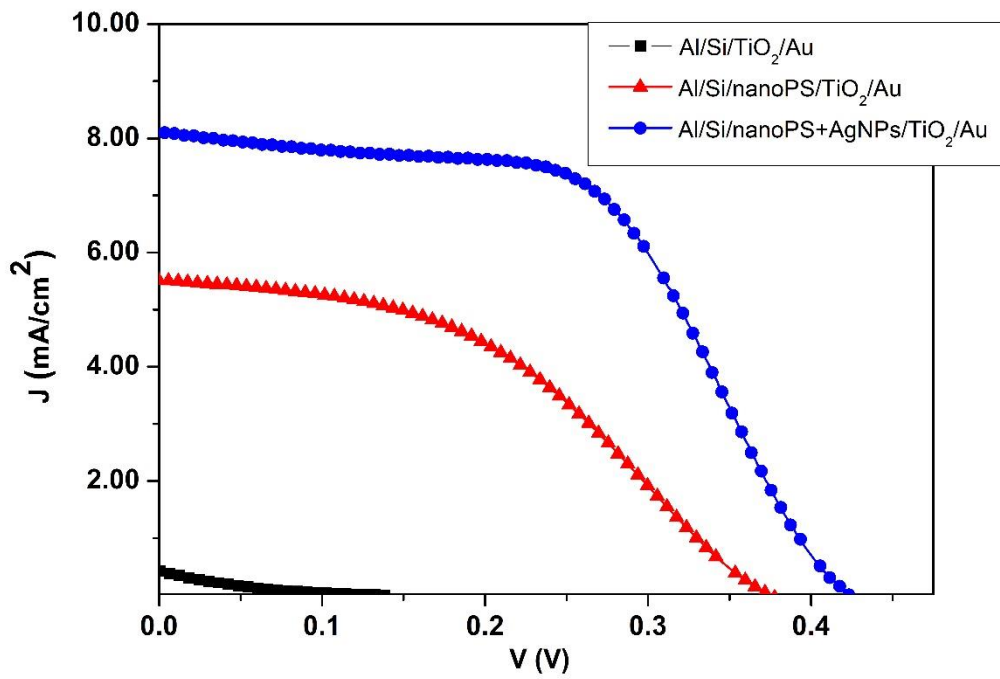


Figure 8. J - V characteristic of $\text{Al/Si/TiO}_2/\text{Au}$, $\text{Al/Si/nanoPS/TiO}_2/\text{Au}$ and $\text{Al/Si/nanoPS+AgNPs/TiO}_2/\text{Au}$ photovoltaic devices.

Table 1: Photovoltaic characteristics of the three MIS Schottky solar cells under study.

Device structure	J_{sc} (mA/cm^2)	V_{oc} (V)	FF	η (%)
Al/Si/TiO₂/Au	0.43	0.14	13.5	0.008
Al/Si/nanoPS/TiO₂/Au	5.52	0.38	42.7	0.9
Al/Si/nanoPS+AgNPs/TiO₂/Au	8.07	0.42	55.9	1.9

Figure 9 shows the maximum power density values for the three devices, which allows to calculate the fill factor (FF) and efficiency (η) from the following well-known relations [12, 52]:

$$FF = \frac{I_m V_m}{I_{sc} V_{oc}} \quad (1)$$

$$\eta = \frac{P_{out}}{S \cdot P_{in}} = \frac{I_m V_m}{S \cdot P_{in}} \quad (2)$$

where, $I_m V_m$ is the maximum power point, S is the active area of the solar cell and P_{in} is the power density of the incident light (100 mW/cm^2).

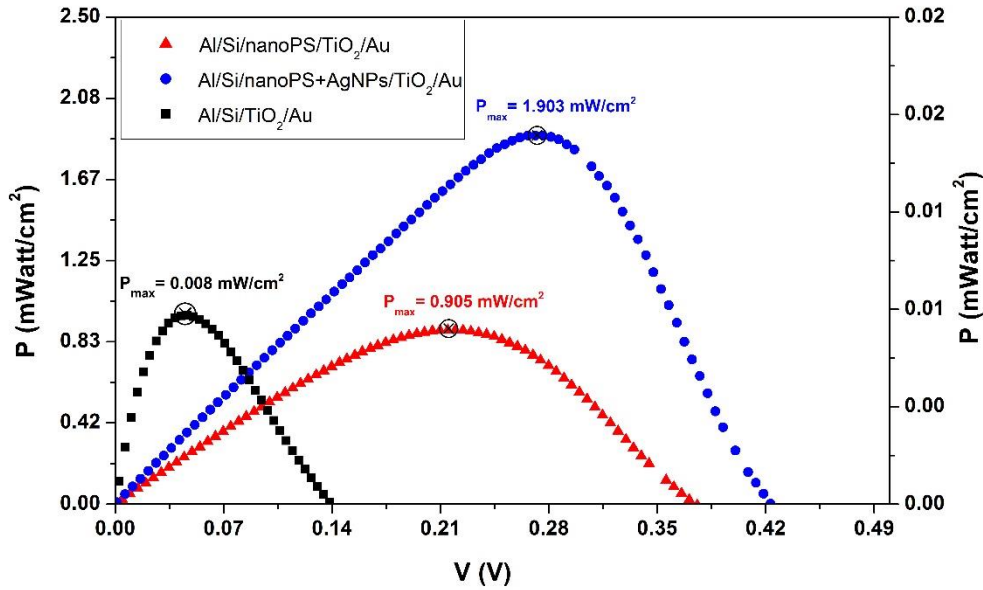


Figure 9. Maximum power density point determination for the Al/Si/TiO₂/Au, Al/Si+naoPS/TiO₂/Au, and Al/Si/nanoPS+AgNPs/TiO₂/Au photovoltaic devices.

It is important to mention that the addition of TiO₂ thin films to the Schottky junction devices has several advantages. First of all, they serve as interfacial layers to improve V_{oc} by hole blocking and electron transportation. As a result of the wide band gap of the TiO₂ thin films (3.82 eV, section 3.2.1), the TiO₂/active layer interfaces are expected to have a large valence-band barrier ($\Delta E_v \sim 2.5 \text{ eV}$), which would block the transport of holes from

the active layer to the TiO₂ thin film. However, these interfaces are expected to possess a small conduction-band barrier ($\Delta E_c \sim 0.1$ eV), which would allow transport of electrons from the active layer to the TiO₂ thin film [43] (see energy band diagrams, Fig. 6). Second, the TiO₂ thin films serve as antireflective coatings. Third, the TiO₂ thin films passivate the surface of the active layer and prevent it from oxidation, in addition to the notable reduction in surface recombination rates associated to nanoPS. This enhancement was observed from the photovoltaic parameters for the Al/Si/nanoPS/TiO₂/Au and Al/Si/nanoPS+AgNPs/TiO₂/Au devices. Finally, in the case of the latter devices, which have shown the highest efficiency, the interaction between TiO₂ (dielectric layer) with AgNPs led to an enhancement in the optoelectronic properties due to the manifestation of SPR effects in the blue region of the electromagnetic spectrum (Fig. 4).

In conclusion, the optoelectronic enhancement for the Al/Si/nanoPS+AgNPs/TiO₂/Au devices shown in Figs. 7 and 8 is attributed to five main factors: (1) Reduction in the recombination rates by improving surface passivation, (2) improved light trapping by the use of TiO₂ thin film as antireflective coating, (3) increased light absorption by the nanoPS layer, (4) SPR effects associated to the presence of AgNPs, and (5) improved electrical conduction of the active layer by the presence of AgNPs.

Finally, it is worth pointing out that the results here presented are comparable to those obtained for several Schottky barrier junction solar cells based on crystalline Si and low-dimensional structures. For example, $J_{sc} = 0.396$ mA/cm² and $V_{oc} = 0.429$ V have recently been obtained for Schottky junction solar cell based on Si nanowires and multi-layered graphene after optimizing the number of graphene layers [53], $\eta = 1.25\%$ was obtained for Schottky junction solar cells based on patterned graphene and CdS nanobelts [54], $\eta = 1.65\%$ for Au-graphene/(CdS nanowires) Schottky junction solar cells [55], and plasmonic enhancement in MIS Schottky junction solar cells by introducing Ag NPs and SiO_x spacer layers on top of the junction, where J_{sc} improved from 13.7 mA/cm² for the reference cell to 19.7 mA/cm² after optimizing the size, shape and distributions of Ag NPs [56].

4. CONCLUSIONS

We have analyzed in detail the optoelectronic performance of three different MIS Schottky junction solar cells, namely Al/Si/TiO₂/Au, Al/Si/nanoPS/TiO₂/Au, and Al/Si/nanoPS+AgNPs/TiO₂/Au structures. A remarkable improvement in the photovoltaic performance of the devices was found upon the addition of nanoPS and AgNPs. To understand the different photogeneration and conduction mechanisms, an energy band model was proposed for the different devices.

The large increase in the overall photovoltaic performance of the Al/Si/nanoPS+AgNPs/TiO₂/Au devices is attributed to two main reasons, in addition to the reflectance reduction and the passivation provided by the nanoPS layers. First, the small size of the AgNPs (5-15 nm) leads to the manifestation of SPR effects in the blue region of the electromagnetic spectrum. Second, the metallic AgNPs improved the electrical conduction of the nanoPS layers.

It is worth pointing out that the growth of TiO₂ thin films most likely does not completely passivate the surface of nanoPS due to the presence of small meso-pores (5-30 nm). As such, radiative recombination mechanisms through oxygen vacancies in the small nanopores of the surface of nanoPS still may exist for the Al/Si/nanoPS/TiO₂/Au devices. However, surface passivation of nanoPS was highly improved by the chemical process used for the infiltration of silver nanoparticles leading to the Al/Si/nanoPS+AgNPs/TiO₂/Au structures.

5. Conflicts of Interest disclosures

Funding. Egyptian ministry of higher education, missions section under Egyptian joint supervision Grant, call 015/016.

Acknowledgments. The authors are thankful to Mr. Luis García Pelayo and Dr. Valentin Constantin Nistor for technical support.

Disclosures. The authors declare no conflicts of interest.

6. REFERENCES

- 546 [1] Nelson J (2003) *The physics of solar cells*, World Scientific Publishing Company.
- 547 [2] de la Morena SS, Recio-Sánchez G, Torres-Costa V, and Martín-Palma R (2014) Hybrid
- 548 gold/porous silicon thin films for plasmonic solar cells, *Scripta Materialia* 74:33-37.
- 549 [3] Zhou L, Xiao L, Yang H, Liu J, and Yu X (2018) Greatly Enhanced Photovoltaic Performance of
- 550 Crystalline Silicon Solar Cells via Metal Oxide, *Nanomaterials* 8:505.
- 551 [4] Wang X, Peng KQ, Pan XJ, Chen X, Yang Y, Li L, Meng XM, Zhang WJ, and Lee ST (2011) High-
- 552 Performance Silicon Nanowire Array Photoelectrochemical Solar Cells through Surface
- 553 Passivation and Modification, *Angewandte Chemie International Edition* 50:9861-9865.
- 554 [5] Garnett E, and Yang P (2010) Light trapping in silicon nanowire solar cells, *Nano letters*
- 555 10:1082-1087.
- 556 [6] Peng KQ, and Lee ST (2011) Silicon nanowires for photovoltaic solar energy conversion,
- 557 *Advanced Materials* 23:198-215.
- 558 [7] Jasim KE (2015) Quantum dots solar cells, *Solar Cells-New Approaches and Reviews*
- 559 [8] Kim JH, Shin DH, Lee HS, Jang CW, Kim JM, Seo SW, Kim S, and Choi S-H (2017)
- 560 Enhancement of efficiency in graphene/porous silicon solar cells by co-doping
- 561 graphene with gold nanoparticles and bis (trifluoromethanesulfonyl)-amide, *Journal of*
- 562 *Materials Chemistry C* 5:9005-9011.
- 563 [9] Dewan R, Jovanov V, Hamraz S, and Knipp D (2014) Analyzing periodic and random textured
- 564 silicon thin film solar cells by Rigorous Coupled Wave Analysis, *Scientific reports*
- 565 4:6029.
- 566 [10] Schneider BW, Lal NN, Baker-Finch S, and White TP (2014) Pyramidal surface textures for
- 567 light trapping and antireflection in perovskite-on-silicon tandem solar cells, *Optics*
- 568 *express* 22:A1422-A1430.
- 569 [11] Farhat M, Kais S, and Alharbi F (2017) Plasmonically enhanced Schottky photovoltaic
- 570 devices, *Scientific reports* 7:14253.
- 571 [12] Pulfrey DL (1978) MIS solar cells: A review, *IEEE Transactions on Electron Devices* 25:1308-
- 572 1317.
- 573 [13] Shewchun J, Burk D, and Spitzer MB (1980) MIS and SIS solar cells, *IEEE Transactions on*
- 574 *Electron Devices* 27:705-716.
- 575 [14] Sharma B (2013) *Metal-semiconductor Schottky barrier junctions and their applications*,
- 576 Springer Science & Business Media.
- 577 [15] Martín-Palma RJ, McAtee PD, Ramadan R, and Lakhtakia A (2019) Hybrid Nanostructured
- 578 porous silicon-silver Layers for Wideband optical Absorption, *Scientific reports* 9:7291.
- 579 [16] Harizi A, Laatar F, and Ezzaouia H (2019) Physical properties enhancement of porous
- 580 silicon treated with In₂O₃ as a antireflective coating, *Results in Physics* 12:1716-1724.
- 581 [17] Iatsunskiy I, Pavlenko M, Viter R, Jancelewicz M, Nowaczyk G, Baleviciute I, Załęski K, Jurga
- 582 S, Ramanavicius A, and Smyntyna V (2015) Tailoring the structural, optical, and
- 583 photoluminescence properties of porous silicon/TiO₂ nanostructures, *The Journal of*
- 584 *Physical Chemistry C* 119:7164-7171.
- 585 [18] Schmidt J, Kerr M, and Cuevas A (2001) Surface passivation of silicon solar cells using
- 586 plasma-enhanced chemical-vapour-deposited SiN films and thin thermal SiO₂/plasma
- 587 SiN stacks, *Semiconductor Science and Technology* 16:164.
- 588 [19] Titova V, Veith-Wolf B, Startsev D, and Schmidt J (2017) Effective passivation of crystalline
- 589 silicon surfaces by ultrathin atomic-layer-deposited TiO_x layers, *Energy Procedia*
- 590 124:441-447.
- 591 [20] Schmidt J, Veith B, and Brendel R (2009) Effective surface passivation of crystalline silicon
- 592 using ultrathin Al₂O₃ films and Al₂O₃/SiN_x stacks, *physica status solidi (RRL)–Rapid*
- 593 *Research Letters* 3:287-289.
- 594 [21] von Roedern B (2001) How do buffer layers affect solar cell performance and solar cell
- 595 stability?, *MRS Online Proceedings Library Archive* 668:

- [22] Lee Y-T, Lin F-R, Lin T-C, Chen C-H, and Pei Z (2016) Low-temperature, chemically grown titanium oxide thin films with a high hole tunneling rate for Si solar cells, *Energies* 9:402.
- [23] Elshorbagy MH, Cuadrado A, and Alda J (2017) High-sensitivity integrated devices based on surface plasmon resonance for sensing applications, *Photonics Research* 5:654-661.
- [24] Steiner P, Kozlowski F, Wielunski M, and Lang W (1994) Enhanced blue-light emission from an indium-treated porous silicon device, *Japanese journal of applied physics* 33:6075.
- [25] Andsager D, Hilliard J, and Nayfeh MH (1994) Behavior of porous silicon emission spectra during quenching by immersion in metal ion solutions, *Applied physics letters* 64:1141-1143.
- [26] Hosny M, Wissem D, Ikbel H, and Hatem E (2014) Influence of gold nanoparticles deposition on porous silicon properties, *Sensors & Transducers* 27:202.
- [27] Liu K, Bi Y, Qu S, Tan F, Chi D, Lu S, Li Y, Kou Y, and Wang Z (2014) Efficient hybrid plasmonic polymer solar cells with Ag nanoparticle decorated TiO₂ nanorods embedded in the active layer, *Nanoscale* 6:6180-6186.
- [28] Langlet M, Jenouvrier P, Kim A, Manso M, and Valdez MT (2003) Functionality of Aerosol-Gel Deposited TiO₂ Thin Films Processed at Low Temperature, *Journal of sol-gel science and technology* 26:759-763.
- [29] Ramadan R, Romera D, Carrascón RD, Cantero M, Aguilera-Correa J-J, García Ruiz JP, Esteban J, and Silván MM (2019) Sol–Gel-Deposited Ti-Doped ZnO: Toward Cell Fouling Transparent Conductive Oxides, *ACS omega* 4:11354-11363.
- [30] Martín-Palma R, Pascual L, Herrero P, and Martínez-Duart J (2002) Direct determination of grain sizes, lattice parameters, and mismatch of porous silicon, *Applied physics letters* 81:25-27.
- [31] Martín-Palma R, Pascual L, Herrero P, and Martínez-Duart J (2005) Monte Carlo determination of crystallite size of porous silicon from x-ray line broadening, *Applied Physics Letters* 87:211906.
- [32] Torres-Costa V, and Martín-Palma R (2010) Application of nanostructured porous silicon in the field of optics. A review, *Journal of materials science* 45:2823-2838.
- [33] Ramadan R, and Martín-Palma RJ (2019) AC & DC electrical conduction of the interfaces of MIS Schottky barrier diodes based on silicon nanostructures and Ag nanoparticles., *Submitted*
- [34] Chau Y-FC, Chao C-TC, Chiang H-P, Lim CM, Voo NY, and Mahadi AH (2018) Plasmonic effects in composite metal nanostructures for sensing applications, *Journal of Nanoparticle Research* 20:190.
- [35] Mock J, Barbic M, Smith D, Schultz D, and Schultz S (2002) Shape effects in plasmon resonance of individual colloidal silver nanoparticles, *The Journal of Chemical Physics* 116:6755-6759.
- [36] McLachlan D, Priou A, Chenierie I, Issac E, and Henry F (1992) Modeling the permittivity of composite materials with a general effective medium equation, *Journal of Electromagnetic Waves and Applications* 6:1099-1131.
- [37] Mackay TG, and Lakhtakia A (2006) Percolation thresholds in the homogenization of spheroidal particles oriented in two directions, *Optics communications* 259:727-737.
- [38] Watanabe R, Eguchi Y, Yamada T, and Saito Y (2015) Optical properties of spin-coated TiO₂ antireflection films on textured single-crystalline silicon substrates, *International Journal of Photoenergy* 2015:
- [39] Kelly KL, Coronado E, Zhao LL, and Schatz GC. (2003) The optical properties of metal nanoparticles: the influence of size, shape, and dielectric environment, ACS Publications.
- [40] Ramadan R, Abdelhady K, Manso-Silván M, Torres-Costa V, and Martín-Palma RJ (2019) Microwave plasma and rapid thermal processing of indium-tin oxide thin films for

- enhancing their performance as transparent electrodes, *Journal of Photonics for Energy* 9:034001.
- [41] Chrysicopoulou P, Davazoglou D, Trapalis C, and Kordas G (1998) Optical properties of very thin (< 100 nm) sol–gel TiO₂ films, *Thin Solid Films* 323:188-193.
- [42] Zhao B-X, Zhou J-C, and Rong L-Y (2010) Microstructure and optical properties of TiO₂ thin films deposited at different oxygen flow rates, *Transactions of Nonferrous Metals Society of China* 20:1429-1433.
- [43] Avasthi S, McClain WE, Man G, Kahn A, Schwartz J, and Sturm JC (2013) Hole-blocking titanium-oxide/silicon heterojunction and its application to photovoltaics, *Applied Physics Letters* 102:203901.
- [44] Shin DH, Kim JH, Kim JH, Jang CW, Seo SW, Lee HS, Kim S, and Choi S-H (2017) Graphene/porous silicon Schottky-junction solar cells, *Journal of Alloys and Compounds* 715:291-296.
- [45] Gallach-Pérez D, Muñoz-Noval A, García-Pelayo L, Manso-Silván M, and Torres-Costa V (2017) Tunnel conduction regimes, white-light emission and band diagram of porous silicon–zinc oxide nanocomposites, *Journal of Luminescence* 191:107-111.
- [46] Hsu C-H, Lo H-C, Chen C-F, Wu CT, Hwang J-S, Das D, Tsai J, Chen L-C, and Chen K-H (2004) Generally applicable self-masked dry etching technique for nanotip array fabrication, *Nano letters* 4:471-475.
- [47] Dzhaifarov T (2013) Silicon solar cells with nanoporous silicon layer, *Solar Cells-Research and Application Perspectives* 42.
- [48] Al-Douri Y, Ahmed N, Bouarissa N, and Bouhemadou A (2011) Investigated optical and elastic properties of Porous silicon: Theoretical study, *Materials & Design* 32:4088-4093.
- [49] Thiel FL, and Ghandhi SK (1970) Electronic properties of silicon doped with silver, *Journal of Applied Physics* 41:254-263.
- [50] Pascual Sánchez D. (2015) Crystalline silicon Heterojunction solar cells, Universitat Politècnica de Catalunya.
- [51] Martín-Palma R, Pérez-Rigueiro J, and Martínez-Duart J (1999) Study of carrier transport in metal/porous silicon/Si structures, *Journal of Applied Physics* 86:6911-6914.
- [52] Sze SM, and Ng KK (2006) *Physics of semiconductor devices*, John wiley & sons.
- [53] Lin Y-K, Hong Y-T, Shyue J-J, and Hsueh C-H (2019) Construction of Schottky junction solar cell using silicon nanowires and multi-layered graphene, *Superlattices and Microstructures* 126:42-48.
- [54] Ye Y, Gan L, Dai L, Dai Y, Guo X, Meng H, Yu B, Shi Z, Shang K, and Qin G (2011) A simple and scalable graphene patterning method and its application in CdSe nanobelt/graphene Schottky junction solar cells, *Nanoscale* 3:1477-1481.
- [55] Ye Y, Dai Y, Dai L, Shi Z, Liu N, Wang F, Fu L, Peng R, Wen X, and Chen Z (2010) High-performance single CdS nanowire (nanobelt) Schottky junction solar cells with Au/graphene Schottky electrodes, *ACS applied materials & interfaces* 2:3406-3410.
- [56] Tong C, Yun J, Song H, Gan Q, and Anderson WA (2014) Plasmonic-enhanced Si Schottky barrier solar cells, *Solar Energy Materials and Solar Cells* 120:591-595.